Controlling the electronic band structures in hydrogenated silicon nanocrystals by shallow impurity doping

X. Y. Chen and W. Z. Shen*
Laboratory of Condensed Matter Spectroscopy and Opto-Electronic Physics, Department of Physics, Shanghai Jiao Tong University, 1954 Hua Shan Road, Shanghai 200030, People's Republic of China
(Received 24 September 2004; published 6 July 2005)

By the aid of magnetic-field-dependent Hall effect measurements, we have extracted the electron mobility and concentration in hydrogenated Si nanocrystals grown on crystalline silicon substrates within the framework of mobility spectrum analysis. A unified model based on diffusive and ballistic transport mechanisms has been employed to explain the observed electron mobility in Si nanocrystals with different doping levels, as well as the mobility edge in low-doping Si nanocrystals. Both the theoretical and experimental results clearly demonstrate the control of the electronic band structures by shallow impurity phosphorus doping in Si nanocrystals, which provide an experimental basis for further nanoelectronic device design using Si nanocrystals.

DOI: 10.1103/PhysRevB.72.035309 PACS number(s): 73.63.Kv, 72.20.Fr, 72.20.Ee, 74.20.De

I. INTRODUCTION

Due to the three-dimensional confinement of electrons (or holes) in nanocrystals or quantum dots, significant modifications of the optical and electronic properties, including the widely studied strong increase of the optical transition energies, are expected as compared to those of bulk materials.[1] It is well known that shallow donors (or acceptors) are crucial in determining the transport properties in bulk semiconductors, while, for doped quantum dot systems, the impurity doping will also change the electronic band structures of the nanocrystals greatly. Therefore, it is interesting to investigate how the electronic states of shallow impurities are modified and what the different electronic transport properties are in highly confined doped systems.

However, there is still a lack of experimental studies addressing these issues, mainly due to the difficulties in preparation of samples in a controllable manner. Fujii *et al.*[2] have developed a method to grow isolated Si nanocrystals in insulating glass matrices and studied the electronic states of shallow phosphorus donors in these Si nanocrystals. Melnikov and Chelikowsky[3] have performed a theoretical investigation to confirm the observed strong size dependence of the phosphorus hyperfine splitting in electron spin resonance. Nevertheless, it should be noted that carrier transport is prohibited between these isolated Si nanocrystals and the Hall effect is not applicable.[2] In order to observe the electronic transport between Si nanocrystals and investigate the modification of the electronic band structure due to doping, the Si nanocrystals must be close enough together to permit electron transmission.

Recently, we have successfully established a method to obtain a large density of Si grains (10 nm or less in size) separated by very narrow amorphous silicon (*a*-Si) boundaries (about 2–4 atomic spacings in thickness) on crystalline silicon (*c*-Si) substrates by plasma-enhanced chemical vapor deposition (PECVD) under optimal growth conditions.[4,5] The narrow *a*-Si boundaries largely enhance the electron transmission between the Si grains, allowing us to investigate the electronic transport properties by Hall effect measurements.[5] In this kind of Si nanocrystal system, the trapping states at the *a*-Si boundaries cause the depletion of electrons in the Si grains, resulting in the formation of different electronic band structures with three-dimensional potential wells, where the electrons are localized. The electron depletion in the Si grains will be strongly related to the donor (or acceptor) concentration. As a result, in contrast to the bulk *c*-Si case, shallow impurity doping in the Si nanocrystal system is expected to control the electronic band structure, which can be revealed by barrier scattering on mobility. The modification of electronic band structures is very significant for the improvement of nanoelectronic devices, as well as the realization of electron localization in the Si grains.

In this paper, we demonstrate the control of the electronic band structure by shallow impurity doping in Si nanocrystals grown by PECVD on *c*-Si substrates. The transport parameters of the Si nanocrystals have been obtained from the phosphorus-doped Si nanocrystal/*c*-Si structures through a mobility spectrum analysis (MSA),[6–8] following variable-magnetic-field Hall effect measurements. The results on electron mobility and concentration are explained well by a unified model including diffusive and ballistic transport mechanisms. The variation of the electron barrier height has been further verified by the observation of the mobility edge in the Mott transition and the exponential temperature-dependent behavior of the electron mobility in differently doped samples.

The paper is arranged as follows. In Sec. II, we introduce the growth conditions and experimental details for the studied samples. In Sec. III, the unified transport model is introduced and discussed. The experimental results for the electron mobility and their comparison with the calculations are given in Sec. IV. A summary is given in Sec. V.

II. SAMPLE PREPARATION AND EXPERIMENTS

Phosphorus-doped Si nanocrystals have been prepared in a rf (13.56 MHz) capacitively coupled PECVD system from silane (SiH_4) and hydrogen (H_2) on high-purity *c*-Si substrates (both weakly *p* and *n* type) at a temperature of

TABLE I. Doping ratio D_p, film thickness, average grain size s, crystallinity, room-temperature electron mobility μ, average electron concentration $\bar{n}$, and barrier height E_b of Si nanocrystals grown on c-Si substrates.

Sample	c-Si substrate	D_p (%)	Thickness (μm)	Average grain size s (nm)	Crystallinity (%)	μ ($cm^2/V\,s$)	$\bar{n}$ (cm^{-3})	E_b (meV)
C	n type	0	3.1	9.5	57.7	887	1.6×10^{15}	0.6
C1	p type	0.5	4.5	9.3	52.5	760	3.0×10^{15}	1.0
C2	p type	1.0	3.5	7.7	46.8	450	7.9×10^{15}	4.9
C3	p type	5.0	1.4	9.5	47.0	149	2.5×10^{17}	31.3
C4	p type	10.0	0.6	8.4	56.9	23	6.0×10^{18}	73.1

250 °C. The percentage content of silane (SiH_4/SiH_4+H_2) is about 1.0%. Phosphine was used as dopant gas with a percentage content of phosphine D_p (PH_3/SiH_4), ranging from 0 to 10.0%. The Si nanocrystal thin film has a layer thickness of around a few micrometers, as listed in Table I. The structure of these Si nanocrystals has been characterized by x-ray diffraction measurements. The good quality of the Si nanocrystals is indicated by the relatively sharp and symmetric (111) diffraction peak, together with two broad (220) and (311) structures. The average Si grain size s about ~10 nm (see Table I) can be obtained from the width of the (111) diffraction peak by the Scherrer formula. Raman scattering measurements reveal a crystallinity of ~50% in all of those samples, as listed in Table I.

Usually, an electron channel always appears on the surface of highly resistive c-Si substrates due to charged surface states or states in the native oxide layer.[9] Due to the band discontinuity in the heterostructure, the presence of a two-dimensional electron gas (2DEG) at the Si nanocrystal/c-Si interface has been clearly demonstrated by the temperature-dependent electron transport properties and the 2D electronic-state-related tunneling phenomena, as well as the lattice-match-induced ordered microstructures with a good interface.[5] It is obvious that this kind of Si nanocrystal/c-Si heterostructure contains three planar conducting layers: Si nanocrystals, c-Si substrate, and their interfacial 2DEG. These three conducting layers will show different transport parameters (carrier mobility, concentration, and type). On the basis of the distribution of relaxation times with energy and the relationship between conductivity tensors and conductivity concentration functions, the recently developed MSA technique[6–8] has the ability to extract the transport parameters of all carrier species present within the heterostructures. Therefore, we have employed the magnetic-field-dependent Hall effect measurements with a Van der Pauw configuration under an Oxford Instruments superconductive magnet (temperature from 4.2 to 300.0 K and magnetic field up to 15 T), followed by the MSA technique, to extract the transport parameters of all carrier species present within samples that are contributing to the planar conduction process. The details to extract the transport parameters in the Si nanocrystal/c-Si heterostructures can be found in our previous papers.[5]

III. UNIFIED TRANSPORT MODEL

Without considering the electron depletion in the grains, the transport in Si nanocrystals can be regarded as the usual conduction due to different crystallinity. However, in the present Si nanocrystals with extremely narrow a-Si boundaries, the potential barrier is dominated by the electron depletion in the grains. Therefore, we start with an ideal system of uniform grains to discuss the electron transport between silicon grains under zero bias. In the ideal system, we assume that there is only one type of impurity atom present, the impurity atoms are totally ionized and uniformly distributed with a concentration of N_D cm^{-3}. The c-Si energy band structure is also assumed to be applicable inside the grains. The a-Si boundary is of negligible thickness compared to the grain size s, and contains Q_t cm^{-2} of traps located at energy level E_t. Although the real system is a three-dimensional substance, for the purpose of calculating its transport properties, it is sufficient to treat the problem in one dimension. Here, we consider a chain with a length S, which is made up of v grains ($S=vs$). The periodic parabolic energy band profile can be obtained from the solution of the Poisson function, as plotted in Fig. 1(a). E_m is the maximum of the band edge profile $E_C(x)$, the barrier height is $E_b=E_m-E_C(0)$, and the average electron barrier width w is defined as the width of the depletion region at $E_C(x)=[E_m+E_C(0)]/2$, and equals $0.29(s-2d)$. These band structure parameters, as well as the Fermi level E_F at zero bias, can be determined by the donor concentration N_D, trapping energy level E_t, and trapping-state density Q_t, as discussed in Ref. 10.

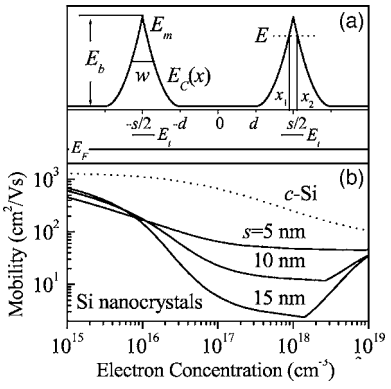

FIG. 1. (a) Schematic equilibrium band edge profile for a nanocrystal with identical grains. (b) Theoretical (from the unified transport model) electron mobility μ vs average concentration $\bar{n}$ in Si nanocrystals with different grain sizes s. The electron mobility of c-Si as a function of concentration n has also been shown as the dotted curve for comparison.

Within the above assumptions, the average electron concentration in the Si nanocrystals can be easily obtained as

$$\bar{n} = \frac{1}{s}\int_{-s/2}^{s/2} N_c \exp\{\beta[E_F - E_C(x)]\}dx$$
$$= N_C \exp\{\beta[E_F - E_C(0)]\} \times\left(\frac{2d}{s} + \frac{s-2d}{2s}\sqrt{\frac{\pi}{\beta E_b}}\mathrm{erf}(\sqrt{\beta E_b})\right), \quad (1)$$

with the parameter $\beta = 1/k_B T$ and the effective density of states in the conduction band $N_C = 2(2\pi m^*/\beta h^2)^{3/2}$. The width d is equal to zero and complete depletion occurs in the grains, when the doping level is low ($sN_D < Q_t$). We note that the expression for the electron concentration in c-Si, i.e., $N_C \exp\{\beta[E_F - E_C(0)]\}$, still holds in Eq. (1), which reflects the improvement of electron concentration in Si nanocrystals with the rise of the Fermi level due to the increase of the donor concentration N_D. Therefore, the average electron concentration $\bar{n}$ is proportional to the donor concentration N_D, but they are not equal due to the electron depletion at the grain boundaries.

The zero-bias conductivity in periodic barrier systems can be expressed as[11]

$$\sigma = \frac{4\pi e^2 l m^*}{\beta h^3}\ln(1 + e^{\beta(E_F - E_m)})\Gamma\frac{vs}{l + \tilde{S} + \tilde{\Lambda}} \quad (2)$$

with

$$\Gamma = 1 + \frac{\beta}{\ln(1 + e^{\beta(E_F - E_m)})}\int_{E_c(0)}^{E_m}\frac{T^{\mathrm{WKB}}(E)}{1 + e^{\beta(E - E_F)}}dE,$$

$$T^{\mathrm{WKB}}(E) = \exp\left(-\frac{2}{\hbar}\int_{x_1}^{x_2}\sqrt{2m^*[E_C(x) - E]}\right),$$

$$\tilde{S} = 2v\Gamma\int_0^{s/2}\frac{\ln(1 + e^{\beta[E_F - E_m]})}{\ln(1 + e^{\beta[E_F - E_C(x)]})}dx,$$

$$\tilde{\Lambda} = 2(v-1)\int_0^{s/2}\left(1 - \Gamma\frac{\ln(1 + e^{\beta[E_F - E_m]})}{\ln(1 + e^{\beta[E_F - E_C(x)]})}\right)e^{-2x/l}dx.$$

Here, l is the electron mean free path. In the WKB tunneling probability $T^{\mathrm{WKB}}(E)$, x_1 and x_2 are the positions of the left and right turning points, respectively, of the electron energy E, as marked in Fig. 1(a). As a result, we can have the electron mobility of the unified model using the terms of diffusive mobility $\mu_e = ev_e\beta l$ and thermionic emission velocity $v_e = (2\pi m^*\beta)^{-1/2}$ in the conductivity of Eq. (2), as the following diffusive transport form with quantum corrections:

$$\mu = \frac{\sigma}{e\bar{n}} = \frac{N_C}{\bar{n}}\ln(1 + e^{\beta(E_F - E_C^m)})\Gamma\frac{vs}{l + \tilde{S} + \tilde{\Lambda}}\mu_e. \quad (3)$$

Furthermore, in order to get a clear physical picture, we consider a low-doping case, where we have the approximations of $d = 0$ and $\ln(1 + e^{\beta(E_F - E_C^m)}) \approx e^{\beta(E_F - E_C^m)}$. By the aid of Eq. (1), the mobility in Eq. (3) can be simplified as

$$\mu = \gamma_1\gamma_2\mu_e, \quad (4)$$

with

$$\gamma_1 = \frac{2}{\sqrt{\pi/\beta E_b}\,\mathrm{erf}[\sqrt{\beta E_b}]}e^{-\beta E_b},$$

$$\gamma_2 = \Gamma\frac{vs}{l + \tilde{S} + \tilde{\Lambda}}.$$

For comparison with the experimental results, we limit our following calculations to the case of $v \to \infty$, where $\gamma_1\gamma_2$ is a function of l, N_D, s, Q_t, and E_t, and reflects the effects of boundary scattering on the diffusive mobility. When the boundary disappears ($\beta E_b \to 0$), $\gamma_1\gamma_2$ approaches 1 and Eq. (4) returns to the diffusive mobility. In fact, Eq. (4) reveals not only the diffusive transport, but also a transition over the mobility edge at $\beta E_b = 1$. It should be noted that the temperature dependence of the mobility is mainly included in the factor γ_1, while γ_2 is a nearly temperature-independent constant. Equation (4) can be further rewritten in two different formats in different temperature regimes:

$$\mu = \begin{cases} \gamma_2\mu_e \propto T^{-\alpha} & \text{for } \beta E_b \ll 1, \\ 2\sqrt{\dfrac{\beta E_b}{\pi}}e^{-\beta E_b}\gamma_2\mu_e \propto e^{-\beta E_b} & \text{for } \beta E_b \gg 1, \end{cases} \quad (5)$$

where α is equal to 3/2 in theory for the ideal lattice scattering,[12] but usually equal to 1 in experiment for $\beta E_b < 1$ near the mobility edge.[13] Equation (5) presents two different temperature-dependent behaviors of the mobility in different temperature regimes, which reveals the Mott transition from lattice scattering in the extended state to barrier scattering in the localized state in the periodic barrier system. Such a transition obtained by the above semiclassical theory has also been predicted in low-dimensional periodic barrier systems by the miniband theory[14] and observed experimentally in GaAs/AlAs semiconductor superlattices.[15] Therefore, this transition is a typical characteristic in periodic barrier systems, and will be demonstrated in our following experimental results in Si nanocrystals.

IV. RESULTS AND DISCUSSION

Figure 1(b) presents the theoretical results [via Eq. (3)] of the electron mobility μ vs average concentration $\bar{n}$ for Si nanocrystals with different grain size s under a trapping state density Q_t of 5.7×10^{12} cm^{-2}. During the calculation, the electron mean free path l in Si nanocrystals has been considered the same as that in bulk c-Si,[11] which can be obtained from the diffusive mobility $\mu_e = ev_e\beta l$, in combination with the electron diffusive mobility in c-Si with a carrier concentration n cm^{-3} of $\mu_e = 65 + 1265/[1 + (n/8.5 \times 10^{16})^{0.72}]$ cm^2/V s.[16] For comparison, we have also shown (the dotted curve) the electron mobility of c-Si as a function of concentration n. It is clear that the electron mobility of the Si nanocrystals is lower than that of c-Si at the same concentration due to the formation of electron barriers. The pronounced

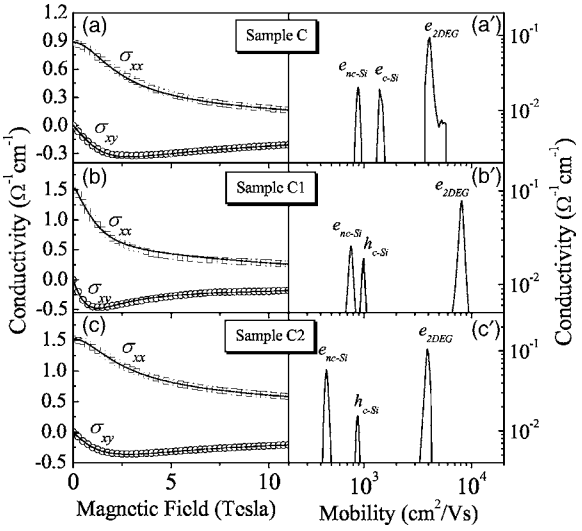

FIG. 2. Experimental (symbols) and theoretical MSA (solid curves) results for the magnetic-field-dependent conductivity tensors (σ_{xx} and σ_{xy}) for sample (a) C, (b) C1, and (c) C2 at room temperature, together with the corresponding mobility spectra shown in (a′), (b′), and (c′).

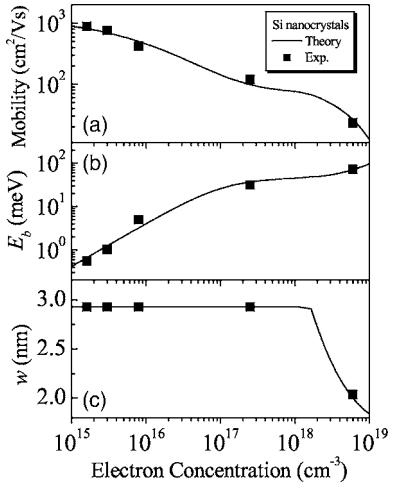

FIG. 3. (a) Room-temperature mobility μ, (b) barrier height E_b, and (c) barrier width w vs average electron concentration $\bar{n}$ in Si nanocrystals. Experimental data, the solid squares; theoretical results from the unified transport model, the solid curves.

mobility minima are associated with the transition from complete depletion of the grains to partial depletion when the donor concentration increases beyond a critical value $sN_D = Q_t$.[10,11] In the low-doping regime of the complete depletion phase ($sN_D < Q_t$), the electron barrier height E_b increases with the donor concentration, resulting in a steep decrease in the electron mobility. However, both the electron barrier height and width will decrease with further increase in the donor concentration in the partial depletion phase ($sN_D > Q_t$) due to the reduction of the depletion region. Furthermore, the increase of grain size s will result in the rapid decrease of the electron mobility in the critical donor concentration region, mainly due to the increase of the electron barrier height via $E_b = e^2 Q_t s / 8\varepsilon$ there (ε is the dielectric permittivity of the c-Si).

Now, let us move to the experimental results on the Si nanocrystals under different phosphorus doping levels. Figures 2(a)–2(c) shows the experimental conductivity tensor components $\sigma_{xx}(B)$ (open squares) and $\sigma_{xy}(B)$ (open circles) as a function of magnetic field B for typical Si nanocrystals at room temperature. Through the successive iterative algorithm in the MSA technique,[6–8] we are able to transform the experimental magnetic-field-dependent Hall data into the dependence of the conductivity density function on mobility, in which each carrier contributing to the total conductivity appears as a separate peak at a given mobility. The transport information of each kind of carrier in the samples has been extracted and is shown as the corresponding mobility spectra in Figs. 2(a′)–2(c′), where each carrier's mobility and concentration can be determined by the peak value and area, respectively. The solid curves in Figs. 2(a)–2(c) are the conductivity tensor components calculated by the MSA. The good agreement between the experiments and calculations clearly demonstrates the reliability of the extracted carrier transport information in the mobility spectra of Figs. 2(a′)–2(c′). The MSA results reveal three kinds of carriers in the studied samples [denoted as $e_{\text{nc-Si}}$, $h_{c\text{-Si}}$ (or $n_{c\text{-Si}}$), and e_{2DEG}], which represent the transport information of the Si nanocrystals, the p-type (or n-type) c-Si substrates, and the 2DEG at the Si nanocrystal/c-Si interfaces, respectively. The detailed assignments of these three carriers can be found in our previous papers.[5] It should be noted that Beck and Anderson[6] have demonstrated convincingly the unique reproduction of the experimental result in terms of the mobility spectra by the aid of the Krein theorem.

Table I lists the yielded room-temperature experimental electron transport parameters (mobility μ and average concentration $\bar{n}$) for the Si nanocrystals with different doping levels. The average concentration $\bar{n}$ of the Si nanocrystals shows nearly an exponential increase with the phosphine doping ratio $D_p(\text{PH}_3/\text{SiH}_4)$, indicating the high doping efficiency and large content of Si grains in the studied Si nanocrystal samples. This experimental result corresponds well with the argument of doping-induced Fermi level rise for Si nanocrystals in Eq. (1), in contrast to the almost doping independence of the electron concentration in a-Si materials. The increase of the doping level not only improves the average electron concentration in the Si nanocrystals, but also causes the electron mobility to deviate from the c-Si diffusive mobility due to the changes of the trapping-state density and electronic band structure, as discussed below.

Figure 3(a) shows the room-temperature experimental (solid squares) electron mobilities μ and average concentrations $\bar{n}$ in the Si nanocrystal samples. From the experimental mobilities μ and average concentrations $\bar{n}$, we can obtain the barrier height E_b and barrier width w through the unified transport model, as presented by the solid squares in Figs. 3(b) and 3(c), respectively. The electron mobility is found to decrease monotonically with the increase of electron concentration, which corresponds to the increase of barrier height E_b and the decrease of barrier width w in the partial depletion regime (w is a constant and equals $0.29s$ in the complete

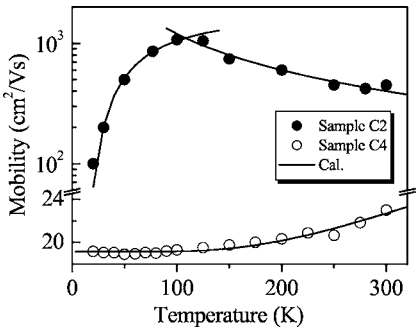

FIG. 4. Temperature-dependent electron mobility of Si nanocrystals. Experimental data, the symbols; theoretical fitting results, the solid curves.

depletion phase of $sN_D < Q_t$). Detailed theoretical calculations show that the trapping-state density Q_t [with $E_t = E_C(0) - 0.18$ eV] in these samples ranges from 1.0×10^{12} to 5.7×10^{12} cm^{-2}, which are reasonable values to reflect the magnitude of the surface state density of c-Si.[10] Moreover, the trapping-state density Q_t is found to increase with donor concentration in Si nanocrystals. These conclusions have also been observed in experiments on microcrystalline[11] and polycrystalline Si.[10] The solid curves in Fig. 3 are the calculated results through the unified transport model with a simple linear relationship between Q_t and N_D:[11] $Q_t = 1.2 \times 10^{12} + 5.4 \times 10^{-7} N_D$ cm^{-2}. It is clear that the theoretical results can well explain the observed variation of electron mobility, barrier height, and width in the Si nanocrystals as a function of the average concentration. Therefore, the electronic band structures and the transport properties of the Si nanocrystals can be really controlled by properly doping shallow impurities.

The following temperature-dependent electron mobility behavior gives further evidence of the observed electron barriers. Figure 4 shows the temperature-dependent Hall mobilities of the low- ($D_p = 1.0\%$ sample C2) and high- ($D_p = 10.0\%$ sample C4) doping Si nanocrystals, as denoted by the solid and open circles, respectively. For the low-doping sample C2, its temperature-dependent mobility displays a clear Mott transition from the band-tail-state conductance (exponential temperature dependence) at $T < 100$ K to the extended-state conductance (power-law temperature dependence) at $T > 100$ K. The mobility results have been fitted very well (the solid curves in Fig. 4) by $\mu = 2.1 \times 10^3 \exp[(-6.0 \text{ meV})/k_B T]$ and $\mu = 1.2 \times 10^5 / T$ cm^2/V s at low and high temperatures, respectively. Such a transition over the mobility edge is in good agreement with the expectation of Eq. (5). Moreover, the yielded electron barrier height of 6.0 meV is in reasonable agreement with the value of 4.9 meV from the unified transport model for this low-doping sample. The exponential decrease of the electron mobility at $T < 100$ K clearly shows the electron localization in Si nanocrystals when the electron potential energy (barrier height) is larger than its low-temperature kinetic energy.

For the high-doping sample C4, the electron mobility is very low due to the high electron barrier height E_b($\sim$73.1 meV), which is much larger than the room-temperature $k_B T$ value of 25.8 meV. Therefore, the above Mott transition over the mobility edge disappears below room temperature, and the temperature-dependent mobility only shows a monotonically decreasing behavior throughout the measured temperature range. It should be noted that the room-temperature electron concentration of this high-doping sample is 6.0×10^{18} cm^{-3}, close to the effective density of states ($N_C = 2.8 \times 10^{19}$ cm^{-3}) in the conduction band of c-Si, indicating the weak degeneration of the Si grains. As a result, impurity band conduction is formed in the system, and the experimental mobility is nearly a constant at $T < 100$ K and increases slightly with increasing temperature at $T > 100$ K.[17] The results in Fig. 4 clearly demonstrate the argument that the experimental mobility can be well described by a function $\mu = 43.3 \exp[(-64.7 \text{ meV})/k_B T] + 19.1$ cm^2/V s, with the two terms corresponding to the barrier (height 64.7 meV) scattering and temperature-independent scattering from the neutralized impurities, respectively. The small deviation of the two barrier heights is due to the weak degeneration in the high-doping sample. A similar weak temperature dependence of the electron mobility and disappearance of the mobility edge below room temperature have also been reported in highly doped microcrystalline Si samples before.[11]

Finally, it should be noted that shallow impurity doping will also have a great effect on the localization of electrons in the Si grains. From the above control of electronic band structures by doping, we can observe that the electron barrier height increases with the donor concentration in the complete depletion region. The increase of barrier height is obviously in favor of electron localization. In the undoped sample C, the barrier height is so small (0.6 meV) that it almost does not influence the electron diffusive transport through the Si grains. In the low-doping sample C2 ($D_p = 1.0\%$), the electron localization can be observed by the appearance of the Mott transition due to the formation of an electronic band structure with suitable barrier shapes. Further evidence of the strong localization comes from the observation of the quantum resonant-tunneling phenomenon in low-doping ($D_p = 0.8\%$) Si nanocrystals.[5] However, delocalization of electrons begins to occur with further increase of the donor concentration, since the high donor concentration results in a large overlap of the electron wave functions in the partial depletion phase, as observed by the formation of impurity band conduction in sample C4 ($D_p = 10.0\%$). Furthermore, the narrow barrier width in the partial depletion region is also a disadvantage for the localization of electrons in Si nanocrystals. Therefore, there is an optimal donor concentration in the low-doping regime, where the electron localization in the Si grains is the strongest.

V. CONCLUSIONS

In summary, we have succeeded in extracting the electron mobility and concentration of phosphorus-doped Si nanocrystals grown on c-Si substrates through variable-magnetic-field Hall effect measurements, followed by a mobility spectrum analysis. The observed electron mobility, barrier height, and barrier width clearly reveal the control of the electronic

band structures by shallow impurity doping in Si nanocrystals, by the aid of a unified model based on diffusive and ballistic transport mechanisms. It is found that there is an optimal donor concentration in the complete depletion regime, where the strongest localization of electrons in Si grains can be reached.

ACKNOWLEDGMENTS

This work was supported in part by the Natural Science Foundation of China under Contract No. 10125416, and Shanghai Municipal Project No. 03DJ14003. The authors would like to acknowledge H. B. Ye for his technical help.

*Corresponding author. Email address: wzshen@sjtu.edu.cn

[1] A. D. Yoffe, Adv. Phys. **50**, 1 (2001).
[2] M. Fujii, A. Mimura, S. Hayashi, Y. Yamamoto, and K. Murakami, Phys. Rev. Lett. **89**, 206805 (2002).
[3] D. V. Melnikov and J. R. Chelikowsky, Phys. Rev. Lett. **92**, 046802 (2004).
[4] Y. L. He, G. Y. Hu, M. B. Yu, M. Liu, J. L. Wang, and G. Y. Xu, Phys. Rev. B **59**, 15352 (1999).
[5] X. Y. Chen and W. Z. Shen, Appl. Phys. Lett. **85**, 287 (2004); X. Y. Chen, W. Z. Shen, and Y. L. He, J. Appl. Phys. **97**, 024305 (2005).
[6] W. A. Beck and J. R. Anderson, J. Appl. Phys. **62**, 541 (1987).
[7] J. R. Meyer, C. A. Hoffman, J. Antoszewski, and L. Raraone, J. Appl. Phys. **81**, 709 (1997).
[8] J. Antoszewski, D. J. Seymour, L. Faraone, J. R. Meyer, and C. A. Hoffman, J. Electron. Mater. **24**, 1255 (1995).
[9] S. M. Sze, *Physics of Semiconductor Devices*, 2nd ed. (Wiley, New York, 1981).
[10] J. Y. W. Seto, J. Appl. Phys. **46**, 5247 (1975).
[11] T. Weis, R. Lipperheide, U. Wille, and S. Brehme, J. Appl. Phys. **92**, 1411 (2002); R. Lipperheide, T. Weis and U. Wille, J. Phys.: Condens. Matter **13**, 3347 (2001).
[12] R. A. Smith, *Semiconductors*, 2nd ed. (Cambridge University Press, London, 1978).
[13] T. Tiedje, J. M. Cebulka, D. L. Morel, and B. Abeles, Phys. Rev. Lett. **46**, 1425 (1981).
[14] S.-R. Eric Yang and S. Das Sarma, Phys. Rev. B **37**, 10090 (1988); H. A. Fertig and S. Das Sarma, *ibid.* **42**, 1448 (1990).
[15] H. T. Grahn, K. von Klitzing, K. Ploog, and G. H. Döhler, Phys. Rev. B **43**, 12094 (1991).
[16] D. M. Caughey and R. E. Thomas, Proc. IEEE **55**, 2192 (1967).
[17] Z. Dziuba, J. Antoszewski, J. M. Dell, L. Faraone, P. Kozodoy, S. Keller, B. Keller, S. P. DenBaars, and U. K. Mishra, J. Appl. Phys. **82**, 2996 (1997).